

Observations of Plasma Upflow in a Warm Loop with Hinode/EIS

Durgesh Tripathi

*Inter-University Centre for Astronomy and Astrophysics, Post Bag 4, Ganeshkhind, Pune
411 007, India*

Helen E. Mason and Giulio Del Zanna

*Department of Applied Mathematics and Theoretical Physics, University of Cambridge,
Wilberforce Road, Cambridge CB3 0WA, UK*

Steven Bradshaw

Department of Physics and Astronomy, Rice University, Houston, TX 77005, USA

ABSTRACT

A complete understanding of Doppler shift in active region loops can help probe the basic physical mechanism involved into the heating of those loops. Here we present observations of upflows in coronal loops detected in a range of temperature temperatures ($\log T = 5.8 - 6.2$). The loop was not discernible above these temperatures. The speed of upflow was strongest at the footpoint and decreased with height. The upflow speed at the footpoint was about 20 km s^{-1} in Fe VIII which decreased with temperature being about 13 km s^{-1} in Fe X, about 8 km s^{-1} in Fe XII and about 4 km s^{-1} in Fe XIII. To the best of our knowledge this is the first observation providing evidence of upflow of plasma in coronal loop structures at these temperatures. We interpret these observations as evidence of chromospheric evaporation in quasi-static coronal loops.

Subject headings: Sun: corona — Sun: atmosphere — Sun: transition region — Sun: UV radiation

1. Introduction

The problem of heating and maintaining the structures in the upper solar atmosphere, such as transition region and corona, has been considered to be one of the most challenging issues in astrophysics. There have been tremendous developments in observations and theory

in the past few decades. However, a definitive solution remains elusive. See Klimchuk (2006) for a review.

The discovery that loop structures are one of the basic building blocks of the solar corona has simplified the problem a great deal to that of understanding the heating and maintenance of individual loops. This is basically because of the inherent characteristics of the corona are such that there is no cross field conduction due to very high electric conductivity.

Recent observations have revealed that active regions comprise different types of loop structures: warm loops (which seem to have a temperature around 1 MK), fan loops (seen emanating from the umbral and penumbral regions at temperatures slightly lower than 1 MK), and hot core loops (seen in the core of active regions at temperatures around 2–3 MK). The heating and maintenance of fan loops and hot core loops are currently a matter of hot debate. For hot core loops, there is evidence for both steady (see e.g., Warren et al. 2008; Brooks and Warren 2009; Warren et al. 2010; Tripathi et al. 2010; Winebarger et al. 2011) as well as impulsive heating (Tripathi, Mason and Klimchuk 2010; Tripathi, Klimchuk and Mason 2011; Viall and Klimchuk 2012; Tripathi, Mason and Klimchuk 2012). However, the observed characteristics of warm loops such as density, filling factors and temperature distribution appear to be consistent with those derived from an impulsive heating model (see e.g., Warren, Winebarger, and Mariska 2003; Tripathi et al. 2009; Ugarte-Urra, Warren, Brooks 2009; Klimchuk 2009, and references therein).

The Doppler shift measurements in previously reported observations of warm loops show predominantly redshifted emission along the loop structures, at around 1 MK (see e.g. Del Zanna 2008; Tripathi et al. 2009). At lower temperatures however, the red shifts are localised towards the footpoints and stronger in magnitude. These downflows (redshifts) are interpreted as plasma radiatively cooling and condensing in the loops (see e.g. Bradshaw 2008; Bradshaw and Cargill 2010). However, the question remains with regard to how this plasma rises up into the loops at first place.

The impulsive heating scenario predicts that the plasma flows up into these loops via the mechanism of chromospheric evaporation which occurs at relatively higher temperatures. Patsourakos and Klimchuk (2006) predict that those high velocity upflows will be clearly seen in Fe XVII lines, or other lines forming at similar temperatures. However, so far there has been no direct detection of these upflows. Such upflows could also be attributed to Type-II spicules (see e.g. De Pontieu et al. 2001).

Here we present the first observations of a warm loop which shows clear upflows of the plasma at low temperatures. These observations are taken with the Extreme-ultraviolet Imaging Spectrometer (EIS; Culhane et al. 2007) aboard Hinode. The paper is structured

as follows. In section 2 we describe the observations followed by data analysis and results in section 3. We summarise and conclude in section 4.

2. Observations

The Extreme-ultraviolet Imaging Spectrometer (EIS; Culhane et al. 2007) onboard Hinode observed an active region, AR 11131, on 11-Dec-2010 using the study sequence which we designed ('GDZ_300x384_S2S3_35'). This sequence uses the 2" slit with an exposure time of 35 seconds. This study sequence is designed to be a sparse raster with a step size of 3". The EIS raster used in this analysis started at 01:55:26 UT and was completed at 02:56 UT. We have applied standard processing software provided in *solarsoft* to the EIS observations.

The left image in Fig. 1 displays a part of the Sun's disk recorded by the 171 Å passband of Atmospheric Imaging Assembly (AIA) onboard the Solar Dynamics Observatory (SDO). The emission in 171 Å passband peaks at a temperature of $\log T=6.0$, similar to the Fe X 184 Å line observed by the EIS. However, depending on the individual structures being observed on the Sun, different channels on AIA may respond differently (see e.g., O'Dwyer et al. 2010; Del Zanna, O'Dwyer and Mason 2011). The over-plotted bigger box shows the area which was rastered by EIS, for which a spectral image built in the Fe X 184 Å is shown in the middle panel. The smaller box in the left panel represent the region which was further studied in detail by AIA. The right panel shows the line-of-sight magnetogram obtained by the Helioseismic and Magnetic Imager (HMI) aboard SDO for the region corresponding to the EIS raster. In the magnetogram, white regions represent the positive magnetic field and dark represent the negative magnetic field regions. AIA and HMI images are taken when the EIS slit would have been approximately at the middle of the raster. It is worthwhile to note that we have coaligned EIS and AIA images just by eye. We believe that the co-alignment is accurate to a level of about 7-8 arc sec. The loop structure, on which this paper is focussed is located by an arrow. These images clearly show that the western footpoint of the loop is rooted in the sunspot seen in the right panel. The eastern moss region corresponding to negative polarity regions is more dispersed. It is worthwhile to note that the moss regions are seen only towards the negative polarity region as noted earlier by Tripathi et al. (2008).

Since we are interested in an understanding of quiescent coronal loops, we analysed the AIA data for about 5 hours (a couple of hours before and after the observations) to make sure that the loop being analysed here was quasi-static and that the active region did not show any flaring and/or micro-flaring activity. Figure 2 displays AIA images recorded in the 171 Å band corresponding to the smaller box shown in the left panel of Fig. 1. It is clear

from these images that there are no major changes in the overall structures of the loops. However, some small variations in the intensity towards the footpoint region can be seen. The results presented here relate to quiescent (1MK) coronal loops seen with TRACE or SDO/AIA at 171 Å.

3. Data Analysis and Results

Figure 3 shows intensity maps derived in Mg V 276 Å, Mg VII 278 Å, Mg VII 280 Å, Fe VIII 186 Å, Fe X 184 Å, Fe XI 188 Å, Fe XII 195 Å, Fe XIII 202 Å and Fe XV 284 Å. As can be seen from these images, the loop structures (shown with arrows in middle left panel) are clearly discernible in Mg VII 278 Å, Si VII 275 Å, Fe IX 188 Å. Only a tiny portion of the loop at footpoint, labelled with an arrow in top row middle panel, is seen in Mg V line. The footpoint of the loop seen in Mg V image is thinner than the same part of the loop seen in other lines such as Si VII and Fe IX. For the higher temperature lines such as Fe X the contrast between loop and the background/foreground fuzzy emission has decreased and it becomes almost impossible to discern the loop in Fe XIII. In other words the corona becomes fuzzier with increasing temperature as was shown with Hinode/EIS data by Tripathi et al. (2009). It is probably worth emphasising that the intensity in the loop structures are just about 10-20% higher than the background/foreground coronal intensities (see e.g. Del Zanna and Mason 2003; Viall and Klimchuk 2012). It is important to note that the intensities in the background/foreground regions are higher in the images obtained in lines like Fe XII and Fe XIII, but decreases in Fe XV. These images also suggest that there are loops at different temperatures intermingled together which can only be distinguished uniquely by spectroscopic observations.

Comparing the structures in AIA images (Fig. 2, spatial resolution ≈ 1 arcsec) and with that in EIS images (Fig. 3, spatial resolution $\approx 3-4$ arcsec) it is clear that the loop structure which appear to be an individual structure in EIS images, comprise several different flux tubes as seen with AIA. A comparison between AIA, EIS and HMI observations reveals that the western footpoints of the loop structures under consideration are rooted in the sunspot (leading polarity) and the eastern footpoints are rooted in more fragmented following polarity magnetic field regions.

The footpoint of the loop, shown by an arrow labelled as 'F' in the left panel in the middle row of the Fig. 3, is brightest. With increasing height, the emission from the loop gets fainter. A closer look at the footpoint region suggests that there are at least three different loops, marked with three arrows higher up, emanating from either the same location or close by. The footpoint regions of these three loops seems to coincide along the line of sight which

could possibly lead to brighter emission near the footpoints.

The two right panels in the top row in Fig. 3 show intensity maps obtained using two lines of Mg VII namely 278 Å and 280 Å. The loop is clearly visible in Mg VII 278 Å, but only a part of the loop is visible in Mg VII 280 Å. We note that the ratio of Mg VII 280 Å to Mg VII 278 Å is sensitive to electron number density. This indicates that the electron density is very low towards the upper part of the loop.

Deriving Doppler shifts from EIS observations is a non-trivial as well as a non-unique process (see e.g. Kamio et al. 2010; Young, O’Dwyer and Mason 2012; Tripathi, Mason and Klimchuk 2012). Most important of all is to remove the orbital variation of the spacecraft and to determine the reference wavelength. Doppler shifts can then be derived. There are a few different ways to derive Doppler shifts from EIS data (see e.g., Kamio et al. 2010; Dadashi, Teriaca and Solanki 2011; Young, O’Dwyer and Mason 2012). In this paper we have used the method proposed by Young, O’Dwyer and Mason (2012). This is based on deriving velocities (using Fe VIII as a reference) in the quiet Sun region of each slit position in the raster. Following this method, we have used the Fe VIII 186.6 Å line in the Quiet Sun to derive Doppler shifts for other lines. We have chosen the bottom 30 rows in the raster be the quiet Sun. The only difference between our method and that of Young, O’Dwyer and Mason (2012) is that they calibrated the quiet Sun using the SUMER measurements from Peter and Judge (1999), whereas we choose the Fe VIII line to have zero Doppler shift, consistent with the new values of Dadashi, Teriaca and Solanki (2011). For more details on this method the reader is referred to Young, O’Dwyer and Mason (2012).

Figure 4 shows the velocity maps derived for Fe VIII, Fe X, Fe XII and Fe XIII. The overall velocity structure in active region appear to be the similar to those published earlier (see e.g. Doschek et al. 2008; Del Zanna 2008; Tripathi et al. 2009), with weakly redshifted core of the active region and strongly blue-shifted low intensity regions. The core of the active region show strong redshifts for the Fe VIII line. This is because the Fe VIII 186 Å line is blended in its redwing with a Ca XIV line which forms at $\log T = 6.4$. Since the core of the active region is characterised by high temperature emission, the Doppler shift for Fe VIII is overestimated. The loop structures marked by arrows in Fig. 3 are blue shifted, unlike the earlier reported observations of strongly redshifted warm loops. The blue shifted loops are marked by arrows in Fig. 4. The loop which is seen along its entire length in blue shifted all along the loop in Fe VIII line and both the foot points are visible. For other spectral lines shown in Fig. 4, only one foot point of the loop is visible and is blue shifted.

To understand the correlation between the loop intensity and its velocity structure better, we plot, intensity and velocity profiles along three different horizontal cuts shown in top left panel of Fig. 5 as ‘Region 1’, ‘Region 2’ and ‘Region 3’. The rest three panels show

the intensity and velocity profiles for three regions. These intensity is plotted for Fe VIII line and the corresponding velocity profiles are plotted for Fe VIII, Fe X, Fe XII and Fe XIII. In the plots, the strong spikes (intensity enhancement) in the intensity profile correspond to the loops marked in Fig. 3. As anticipated the loop intensity decreases with height. Similar characteristics is seen in the velocity profile. The loop is strongly blue shifted at the foot point with a speed of about 20 km s^{-1} in Fe VIII. The velocity of the upflow at the foot point decreases with temperature being about 13 km s^{-1} in Fe X, about 8 km s^{-1} in Fe XII and about 4 km s^{-1} in Fe XIII. In addition, the upflow velocity also decreases with the height of the loop. We note that these speeds are lower limits of the actual speed of the plasma, since we are measuring line-of-site component of speeds. Similar, though less pronounced, characteristics can be seen for other loops adjacent to the strongly emitting loop structure.

The peak of the intensity and velocity profiles for the loops do not coincide with each other. The peak of the velocity seem to be shifted $3''$ eastward with respect to the peak in intensity. This is most likely due to the tilted point spread function of EIS as was pointed out by Young, O'Dwyer and Mason (2012). Young, O'Dwyer and Mason (2012) found that strongly redshifted or blue shifted regions are often seen with some offset from the regions with highest intensity point. Investigating very many different datasets, they concluded that this could be attributed to a tilted point spread function of the instrument. In one observation presented in Young, O'Dwyer and Mason (2012) it was found that there was a difference between intensity peak and velocity peak of $3''$ in Y-direction. In these circumstances, Young, O'Dwyer and Mason (2012) state, "the simplest way of deriving velocity shifts for features with steep intensity gradients is either to study only those pixels at the location of the intensity peaks in the solar-Y direction, or to perform averaging in the Y-direction over a region symmetrically distributed around the intensity peak." In the present observations, even if we average the velocity over the width of the loop in X-direction, the blue shifted pattern remains. Therefore, we conclude that this blue shift seen along the loop is real and not due to some instrumental artifact.

4. Summary and Discussion

We have presented an observation of the active region AR 11131 recorded on 11-Dec-2010 by Hinode EIS. The active region comprises of warm loops, fan loops and hot core loops among other features such as moss etc. The intensity and velocity structure of the active region shows similar characteristics as published earlier by e.g. Doschek et al. (2008); Del Zanna (2008); Tripathi et al. (2009). However, in contrast to the observations reported earlier, where the warm loops at around 1 MK have been shown to be redshifted, the warm

loops in this active region are blue shifted (see Figs 3 and 4). The footpoint of the loop is strongly blue shifted with a speed of about 20 km s^{-1} in Fe VIII. The upflow velocity at the foot point decreases with increasing temperature as well as the height of the loop. To the best of our knowledge this is the first observational report of a blue shifted warm loop.

Based on the multi-stranded impulsive heating scenario, chromospheric evaporation of plasma into coronal loop structures takes place at rather very high temperatures: Patsourakos and Klimchuk (2006) predict high velocity upflows in spectral lines like Fe XVII. In this scenario, the heating takes place in the corona. Energy is conducted downwards leading to chromospheric evaporation into the corona. At the temperature around which lines like Fe VIII would form, most of the strands would be cooling down and therefore the loop emission is expected to be dominated by redshifted emission. So the observations presented here do not seem to show the flow structure expected from this multi-stranded loop models. However, it is important to emphasise here that in these models plasma flow characteristics changes quite significantly when the characteristics of the heating events are changed. The characteristics of the heating events are ad hoc. If the energy of the heating events is significantly higher, then it may well be that high velocity upflows will be seen at higher temperatures and later on the total emission will be dominated by plasma condensation. However, if the energy and duration of heating event is short, the plasma may behave differently and the model may predict upflows at significantly lower temperature, making our observations consistent with an impulsive heating scenario. However, this scenario predicts increasing upflow velocity with temperature, which is opposite to what we observe here.

Our observation is also consistent with the picture that the heating takes place at the foot points of the loops i.e., lower down in the atmosphere rather than higher up in the corona (see e.g. Aschwanden et al 2007). In this scenario too, because of the heat deposition lower down will increase the pressure leading to the plasma evaporation into the loops. If the heat deposition is lower in the atmosphere then evaporation at temperatures of about 1 MK would result in blue shifted emission in the loops, similar to our observations. In fact this is argued to be one of the best evidences for footpoint heating (see e.g. Aschwanden et al 2007).

Lastly, the observations presented here could possibly be consistent with newly proposed mechanism of heating of the solar corona by spicules type II (De Pontieu et al. 20011). In this scenario, the chromospheric material is being pumped into the corona by these spicules and heated.

To the best of our knowledge, these observations present the first clear case of the upflow of plasma in coronal loops and provide an important constraint on the theories of coronal heating. Clearly more observations and theoretical work are needed before anything

conclusive can be said about the heating of warm loops. The future missions such as the Interface Region Imaging Spectrometer (IRIS), the Spectral Imaging of Coronal Environment on board Solar Orbiter and the proposed Large European module for solar Ultraviolet Research (LEMUR) onboard Solar-C will provide with unique and definitive observations to study such problems.

We thank the referee for providing useful inputs which has improved the paper. HEM and GDZ acknowledge STFC. We acknowledge useful discussions at the ISSI on Active Region Heating. Hinode is a Japanese mission developed and launched by ISAS/JAXA, collaborating with NAOJ as a domestic partner, NASA and STFC (UK) as international partners. Scientific operation of the Hinode mission is conducted by the Hinode science team organized at ISAS/JAXA. This team mainly consists of scientists from institutes in the partner countries. Support for the post-launch operation is provided by JAXA and NAOJ (Japan), STFC (U.K.), NASA, ESA, and NSC (Norway).

REFERENCES

- Aschwanden, M. J., Winebarger, A., Tsiklauri, D. and Peter, H. 2007, *ApJ*, 659, 1673
- Bradshaw, S. J. 2008, *A&A*, 486, L5
- Bradshaw, S. J. and Cargill, P. J. 2010, *ApJ*, 717, 163
- Brooks, D. H. and Warren, H. P. 2009, *ApJ*, 703, 10
- Culhane, J. L., Harra, L. K., James, A. M., et al. 2007, *Sol. Phys.*, 243, 19
- Dadashi, N., Teriaca, L., and Solanki, S. K. 2011, *A&A*, 534, 90
- Del Zanna, G., and Mason, H. E. 2003, *A&A*, 406, 1089
- Del Zanna, G. 2008, *A&A*, 481, L49
- Del Zanna, G., O'Dwyer, B., Mason, H. E. 2011, *A&A*, 535, L46
- De Pontieu, B., McIntosh, S. W., Carlsson, M. et al. 2011, *Science*, 331, 55
- Doschek, G. A., Warren, H. P. Mariska, J. T. et al. 2008, *ApJ*, 686, 1362
- Kamio, S., Hara, H., Watanabe, T., Fredvik, T., Hansteen, V. H. 2010, *Sol. Phys.*, 266, 209
- Klimchuk, J. A. 2006, *Sol. Phys.*, 234, 41

- Klimchuk, J. A. 2009 in The Second Hinode Science Meeting: Beyond Discovery-Toward Understanding (ASP Conf. Ser. Vol. 415), ed. B. Lites, et al. (San Francisco: Astron. Soc. Pacific), p. 221
- O’Dwyer, B., Del Zanna, G., Mason, H. E., Weber, M. A., Tripathi, D. 2010, *A&A*, 521, 21
- Patsourakos, S. and Klimchuk, J. A. 2006, *ApJ*, 647, 1452
- Peter, H. and Judge, P. G. 1999, *ApJ*, 522, 1148
- Tripathi, D., Mason, H. E., Young, P. R., Del Zanna, G. 2008, *A&A*, 481, L53
- Tripathi, D., Mason, H. E., Dwivedi, B. N., del Zanna, G., and Young, P. R. 2009, *ApJ*, 694, 1256
- Tripathi, D., Mason, H. E., Del Zanna, G. and Young, P. R. 2010, *A&A*, 518, 42
- Tripathi, D., Mason, H. E., Klimchuk, J. A. 2010, *ApJ*, 723, 713
- Tripathi, D., Klimchuk, J. A., Mason, H. E. 2011, *ApJ*, 740, 111
- Tripathi, D., Mason, H. E., and Kimchuk, J. A. 2012, *ApJ*, arXiv:1204:6550
- Ugarte-Urra, I., Warren, H. P., Brooks, D. H. 2009, *ApJ*, 695, 642
- Viall, N. M., and Klimchuk, J. A. 2012, *ApJ*, arXiv:1202.4001
- Warren, H. P., Winebarger, A. R., and Mariska, J. T. 2003, *ApJ*, 593, 1174
- Warren, H. P. et al. 2008, *ApJ*, 677, 1395
- Warren, H. P., Winebarger, A. R., Brooks, D. H. 2010, *ApJ*, 711, 228
- Warren, H. P., Ugarte-Urra, I., Young, P. R., and Stenborg, G. 2011, *ApJ*, 727, 58
- Winebarger, A. R., DeLuca, E. E. and Golub, L. 2001, *ApJ*, 553, L81
- Winebarger, A. R., Schmelz, J. T.; Warren, H. P.; Saar, S. H.; Kashyap, V. L. 2011, *ApJ*, 740, 2
- Young, P. R., O’Dwyer, B., and Mason, H. E. 2012, *ApJ*, 744, 14

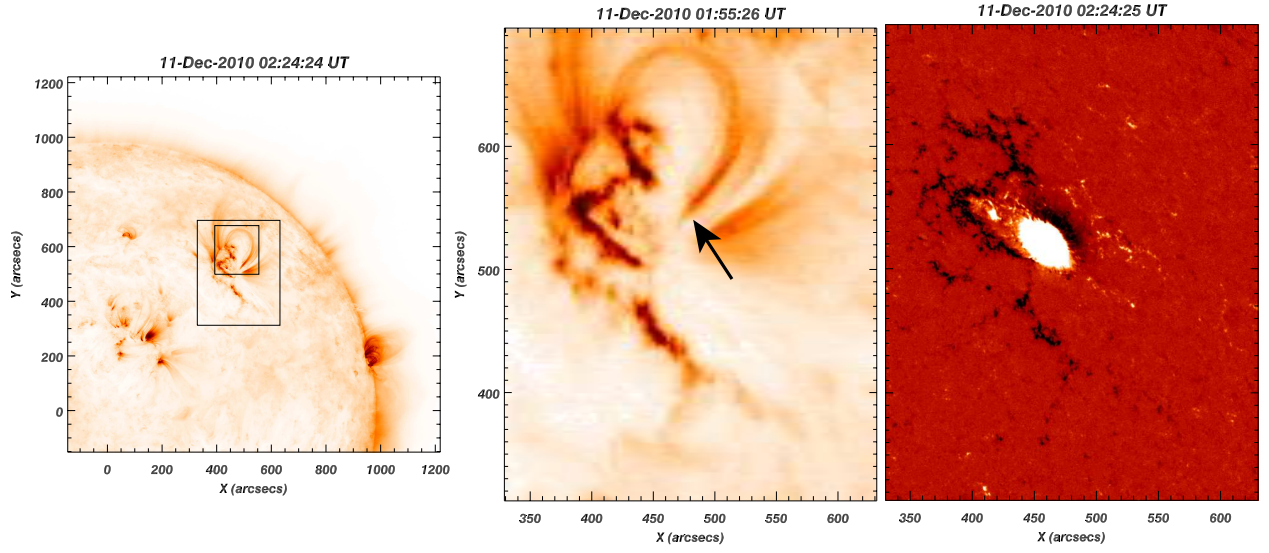


Fig. 1.— Left panel: AIA 171 Å image. The bigger box shows the EIS field of view and smaller box show the region which is studied in detail in Fig. 2. Middle Panel: EIS Fe X image. The arrow locates the foot point of the loop structure which is subject of the study. Right Panel: HMI line of sight magnetic field corresponding to EIS FOV. The magnetic field is scaled between -300 and 300 Gauss.

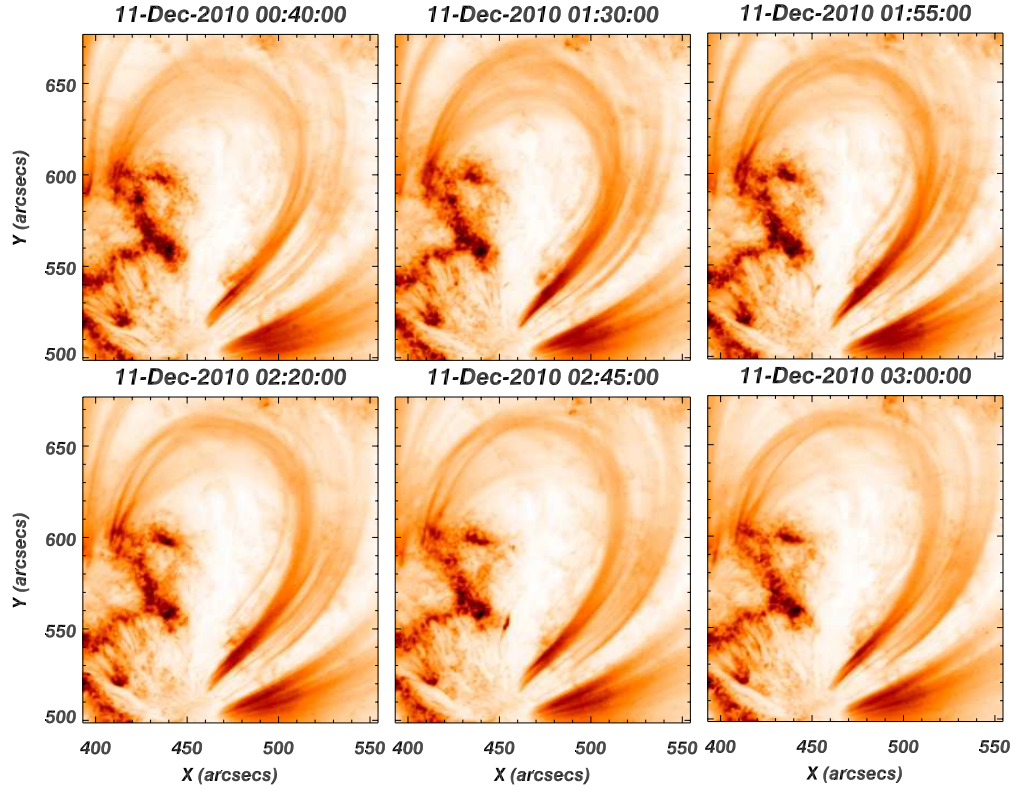


Fig. 2.— AIA 171 Å images corresponding to the small box shown in Figure 1. The images are shown before, during and after the EIS raster.

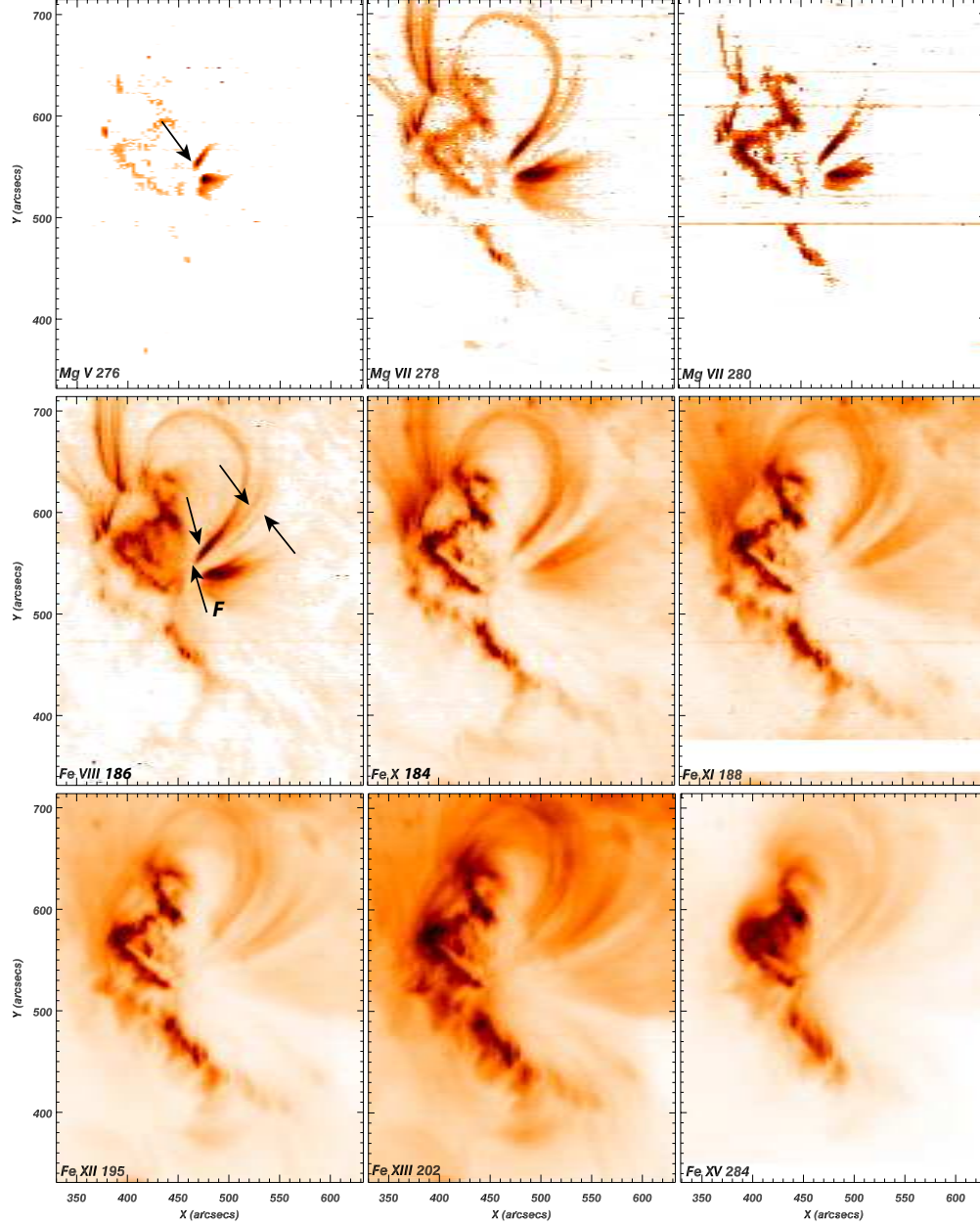


Fig. 3.— Monochromatic intensity maps obtained using EIS spectra. The arrow shown in the top left panel shows the footpoint of the loop seen in Mg V which is also shown by an arrow in top right panel labelled as 'F'. The three arrows shown in the top right panel locate three distinguished loops.

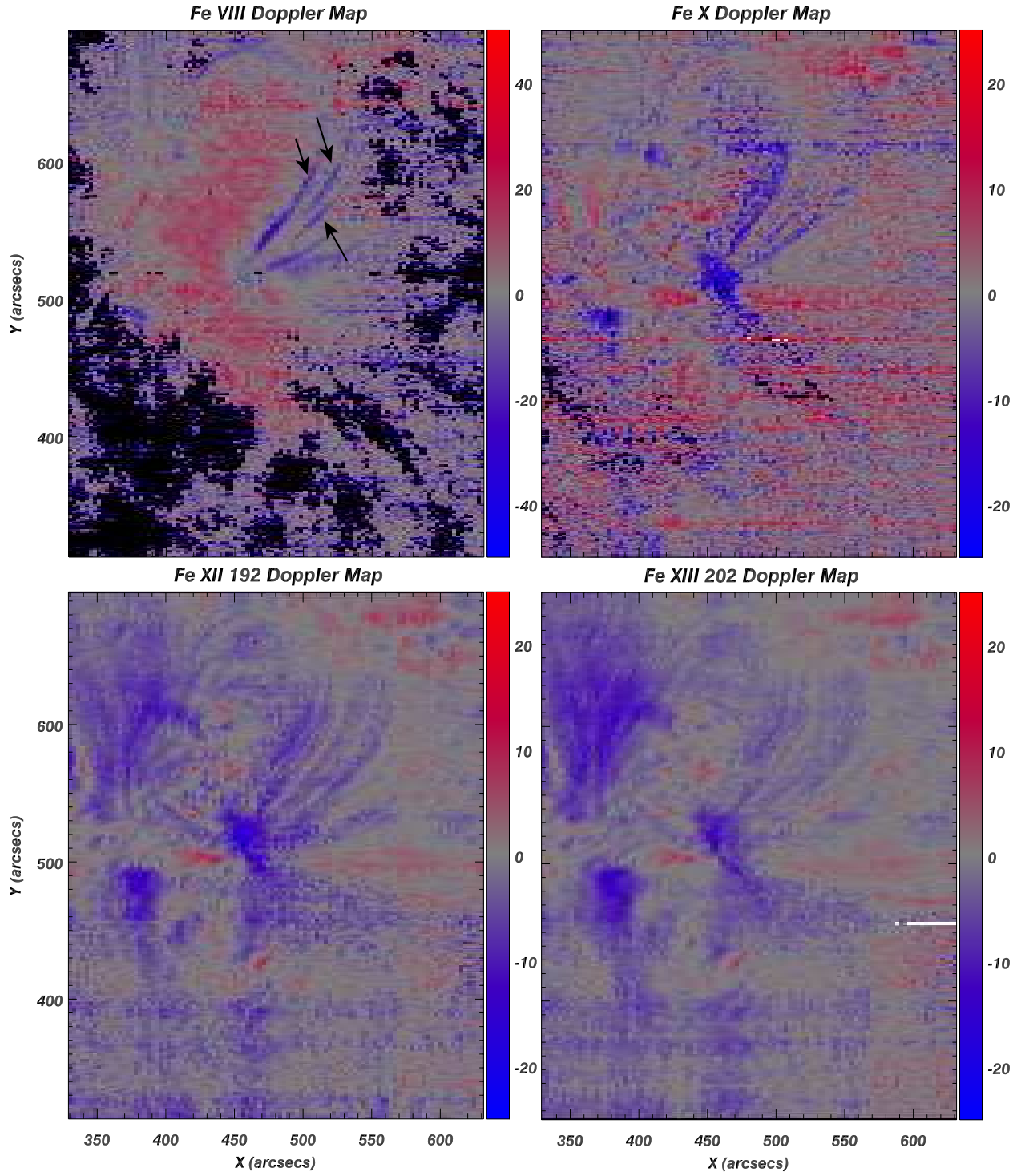


Fig. 4.— Doppler maps for Fe VIII, Fe X, Fe XII and Fe XIII.

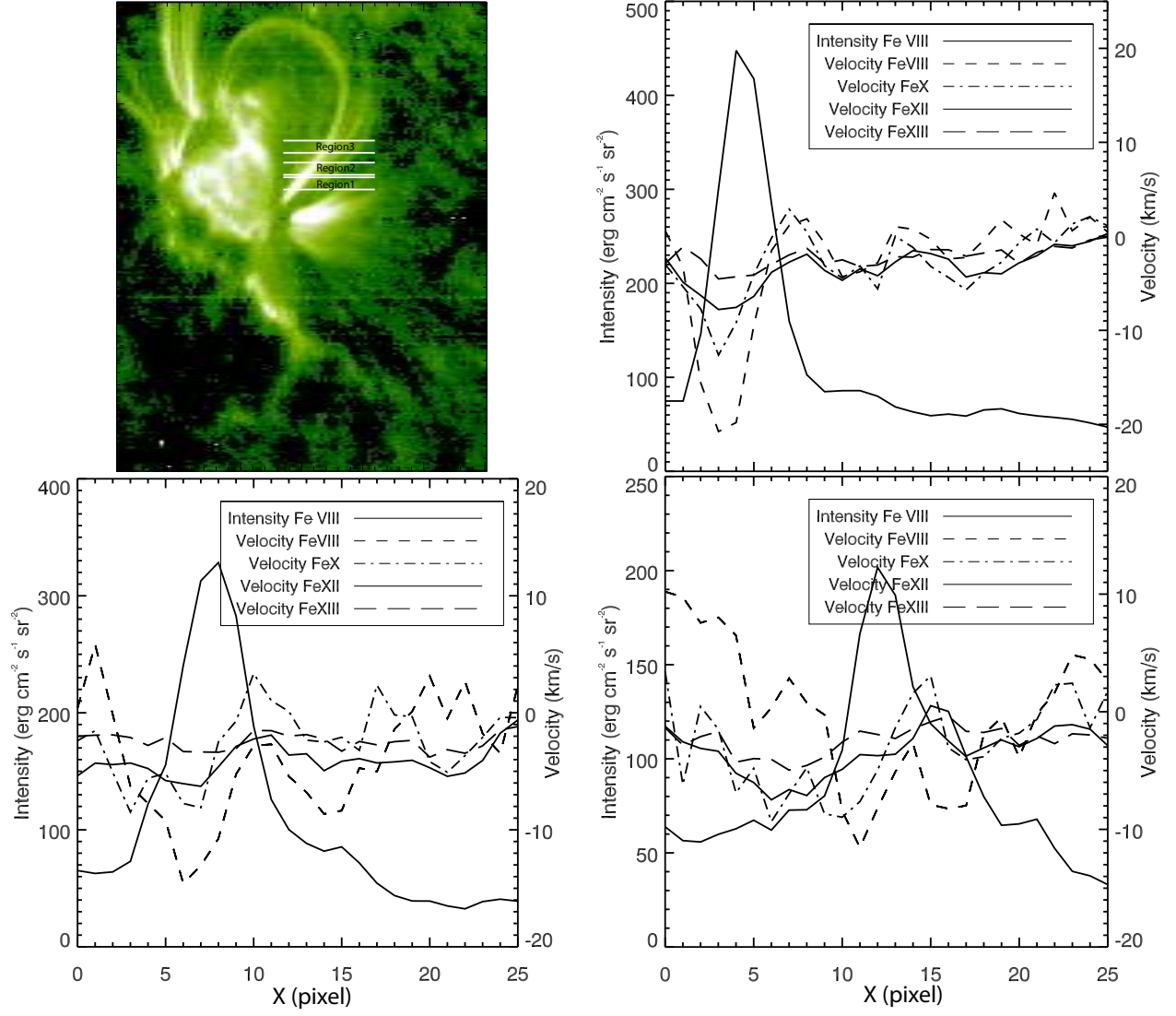


Fig. 5.— Correspondence between Fe VIII intensity profile and velocity profiles for Fe VIII, Fe X, Fe XII and Fe XIII.